The Astrophysical Journal, 769:143 (12pp), 2013 June 1 doi:10.1088/0004-637X/769/2/143

A COMPARISON OF THE INTENSITIES AND ENERGIES OF GRADUAL SOLAR ENERGETIC PARTICLE EVENTS WITH THE DYNAMICAL PROPERTIES OF ASSOCIATED CORONAL MASS EJECTIONS

S. W. Kahler[1] and A. Vourlidas[2]
[1] Air Force Research Laboratory, Space Vehicles Directorate, 3550 Aberdeen Ave., Kirtland AFB, NM 87117, USA; AFRL.RVB.PA@kirtland.af.mil
[2] Space Sciences Division, Naval Research Laboratory, Washington, DC 20375, USA
Received 2012 December 19; accepted 2013 April 19; published 2013 May 15

ABSTRACT

Gradual solar energetic particle (SEP) events observed at 1 AU are produced by shocks driven by coronal mass ejections (CMEs). Characterizations of the remotely imaged CMEs and of their associated SEP events observed in situ can be used to increase our ability to forecast SEP events and to understand better the physical connections between the two phenomena. We carry out a statistical comparison of the peak intensities Ip20, of 120 western-hemisphere 20 MeV SEP events with those of their associated CMEs observed by the *Solar and Heliospheric Observatory*/Large Angle and Spectrometric Coronagraph over the past solar cycle. For a subset of 96 events observed with the EPACT instrument on the *Wind* spacecraft we also compare the SEP 2 MeV peak intensities Ip2, power-law energy spectral exponents γ, total SEP energies Esep, and 2 MeV nuc^{-1} H/He ratios with CME properties. New analyses of white-light CME images enable us to improve calculations of the CME masses and potential energies and then to determine two values of their kinetic energies based on frontal V(fr) and center-of-mass V(cm) speeds. Despite considerable scatter in the SEP and CME data, the large dynamical ranges of both the SEP and CME parameters allow us to determine statistical trends in the comparisons of the logs of the parameters. Ip2, Ip20, and Esep are significantly correlated with CME kinetic energies, masses, and speeds, while γ trends lower (harder). Those correlations are higher with V(fr) than with V(cm) parameters, indicating a less significant role for the body of the CME than for the CME front in SEP production. The high ratios ($\geqslant$10%) of Esep to CME energies found by Mewaldt et al. are confirmed, and the fits are consistent with a linear relationship between the two energies. The 2 MeV nuc^{-1} H/He ratios decrease with increasing CME speeds, which may be an effect of shock geometry. We discuss several factors that limit the estimates of both the SEP and CME energies.

Key words: acceleration of particles – Sun: coronal mass ejections (CMEs) – Sun: flares – Sun: particle emission

1. INTRODUCTION

1.1. SEP Events and CMEs

Gradual $E \geqslant 10$ MeV solar energetic particle (SEP) events are believed to be produced primarily or entirely by acceleration in collisionless shocks driven by fast ($v \geqslant 900$ km s^{-1}) and wide ($W > 60^{\circ}$) coronal mass ejections (CMEs; Gopalswamy et al. 2008a, 2008b; Reames 1999, 2013; Kahler & Reames 2003; Cliver 2009; Li et al. 2012b). Since the CME speeds must be super-Alfvénic to drive shocks, it is not surprising that a correlation between the peak SEP intensities and associated CME speeds has long been known (Kahler 2001), but the scatter is large even in the logs of the peak SEP intensities when compared with observed CME leading-edge speeds (Kahler et al. 1999; Kahler & Vourlidas 2005). Although ground-level events, the most energetic of SEP events, are all associated with the fastest ($v > 2000$ km s^{-1}) CMEs (Gopalswamy et al. 2005b; Mewaldt et al. 2012), some fast CMEs do not produce detectable SEP events (Kahler & Reames 2003; Gopalswamy et al. 2008b), which makes the prediction of SEP events (Crosby 2007; Kahler et al. 2007), important for space weather effects (Bothmer & Zhukov 2007; Guetersloh & Zapp 2010), highly uncertain.

It is clear that the occurrence, and certainly the peak intensity and spectrum of a SEP event, are too complex to be determined by the CME speed alone. The diffusive shock acceleration (DSA) mechanism is the basic process that energizes charged particles (Li et al. 2012b; Reames 2013). The maximum particle energy achieved depends on the seed population, the shock compression ratio, the acceleration timescale (which is dependent on the diffusion coefficient), and the shock dynamic timescale (Li et al. 2012a, 2012b). SEP elemental composition signatures, such as Fe/O and Ne/O, indicate a role for flare particles, either remnant from earlier events or produced in the same flare/CME event, as seed particles in the DSA process (Mewaldt et al. 2012).

These shock and particle variables are not easily observed for remote shocks so the search continues for other observable factors important for SEP production (Kahler et al. 1999, 2000). The intensities of SEP events are enhanced by the presence of previous SEP events (Kahler 2001) and by the interaction of the associated CME with a previously launched wide CME (Gopalswamy et al. 2004; Li et al. 2012b) or with a streamer (Kahler & Vourlidas 2005). In addition, the longitude of the CME source is also a known factor in the SEP timescales (e.g., Cane et al. 1988; Balch 1999; Kahler 2013) and energy spectra (Kahler 2001). Further exploring CME properties, Kahler & Vourlidas (2005) found SEP-rich CMEs to be distinguished from SEP-poor CMEs by their significantly higher masses. Their interpretation of this result was that the higher measured masses were due to CMEs spanning larger ranges of longitude.

1.2. SEP and CME Energies

In an attempt to construct the energy budgets of flare/CME events, Emslie et al. (2004) evaluated the energetics of two large events on 2002 April 21 and July 23. The latter event occurred on the east limb and was not associated with an observed SEP event at 1 AU, but an estimate was made of the total energy of the fluence spectra of the most abundant ions above an energy of 0.001 MeV nuc^{-1} for the 21 April event. The SEP energy

was ∼15% of the CME kinetic energy, which was the dominant component of the released energy in both events. Reassessing this result, Emslie et al. (2005) increased the flare energy budgets of the two events, but the CME kinetic energies were still the dominant components and the SEP ∼15% component was unchanged for the 21 April event.

The SEP–CME energy comparison was extended to five large SEP events observed during the Halloween period of 2003 by Mewaldt et al. (2005a). They measured the fluence spectra from ∼0.1 to several hundred MeV nuc^{-1} for several elements from instruments on the *ACE*, *SAMPEX*, and *GOES* spacecraft. From those measurements they estimated the five SEP event energies and compared them with the CME kinetic energies for the same events determined by Gopalswamy et al. (2005c). In the combined six events the SEP energies of $\sim 10^{31}$ erg were significant fractions (∼0.4%–24%) of the CME kinetic energies. With measurements from the same three spacecraft Mewaldt et al. (2005b, 2005c) selected 11 more large SEP events from 1998 to 2003 for a similar analysis and comparison with published CME kinetic energies (Gopalswamy et al. 2004). The dynamic ranges of the total 17 SEP and CME energies now both extended over two orders of magnitude, but the SEP/CME energy ratios were similar to the earlier results.

In their most recent work Mewaldt et al. (2008) started with the 50 largest SEP events of cycle 23 based on their $E > 30$ MeV fluences and compared the SEP event energies with the 23 available published CME energies (Gopalswamy et al. 2004, 2005c). They calculated the CME kinetic energies in the solar wind (SW) frame by subtracting 400 km s^{-1} from the measured CME speeds and corrected the SEP energies for adiabatic energy losses. The resulting lower CME and higher SEP calculated energies pushed the 23 SEP/CME energy fractions to higher values (mean of 9.5% and median of 6.5%). A recent expansion (Emslie et al. 2012) of the Emslie et al. (2004, 2005) energetics studies of large disk (E60° to W90°) eruptive events included 20 events with SEP and CME energies, 9 of which were included in the Mewaldt et al. (2008) study. Some details of the energetics calculations were changed from the Mewaldt et al. (2008) work, but the log centroids of the 20 events indicated a 0.04 ratio of SEP to CME energies.

These SEP–CME energy comparisons were confined to 23 (Mewaldt et al. 2008) and another 11 (Emslie et al. 2012) large SEP events of the 23rd solar cycle. The calculated energies and masses of the 23 SEP-associated CMEs were all among the largest of the CMEs observed through 2003 (Gopalswamy 2006; Mewaldt et al. 2008). In this work we extend the SEP–CME energetics comparison to include a larger range of SEP event sizes over the entire 23rd solar cycle and a more detailed characterization of the CMEs. We look for any correlations between the SEP events and CMEs that might provide insights into the SEP production and yield predictive tools for SEP event forecasts. The variables involved in this analysis range over several orders of magnitude, so the correlations we perform and the plots shown will be done with logs of the variables, except for the CME speeds. In the discussion below, logs of the parameters will be understood to be the basis of the correlations.

2. DATA ANALYSIS

2.1. Selection of SEP Events and CME Properties

For our analysis we use the Table 1 list of Kahler (2013) of 20 MeV SEP events measured with the EPACT instrument on the *Wind* spacecraft and associated with *Solar and Heliospheric Observatory* (*SOHO*)/Large Angle and Spectrometric Coronagraph (LASCO) CMEs. That event list includes associated flare source locations and has been corrected and updated through 2008. To get the optimum CME mass and speed measurements we limit the events to those observed in the longitude range >W40° to behind the west limb. This yields a total of 120 SEP–CME events over the period 1996–2008.

A comprehensive discussion of the LASCO CME data analysis to convert observed coronagraph brightness to CME mass appears in Vourlidas et al. (2010, 2011). A major concern is that the assumption that each CME lies in the plane of the sky leads to underestimates of their masses, speeds, and energies (Burkepile et al. 2004; Yashiro et al. 2005; Vourlidas et al. 2010), which we address by omitting CMEs from within 40° of the central meridian. Recent work (Colaninno & Vourlidas 2009; Vourlidas et al. 2010; Carley et al. 2012) has also shown that CME masses usually increase until ∼10 $R_\odot$, so that the measurements should be made at or above that height. In 14 cases of our current sample, however, it was necessary to determine the masses below 6 $R_\odot$ where the brightness peaks occurred.

Another problem with past works were the uncertainties for masses and energies for wide (>120°) CMEs, especially for automated measurements like those reported in the CDAW list. These uncertainties have been discussed in Vourlidas et al. (2010) and were the reason for the exclusion of wide events from their statistics. For the same reason, no mass or kinetic energies for halo CMEs are reported in the CDAW list. Wide CMEs are disproportionately associated with large SEP events, so we (A.V.) had to recalculate the masses by hand for the few events in Mewaldt et al. (2005b) and Kahler & Vourlidas (2005). In this paper, we make much more detailed mass measurements over a much larger number of wide/halo CMEs, taking care to avoid both the shock and deflected streamer signatures. Our measurements have, therefore, smaller masses, energies, speeds, and widths, compared to the CDAW catalog. For each sequence of CME images we have calculated the locations, velocities, and accelerations of the centers of mass (cm), as indicated in Figure 1. This allowed us to calculate more realistic CME kinetic energies $E_{\rm kin}$(cm) by summing the velocities over the individual mass elements, as well as the energies $E_{\rm kin}$(fr) that depend on the earlier assumption that the entire CME mass moves at the leading edge (frontal) speed V(fr) (e.g., Gopalswamy et al. 2004, 2005c). From the mass distributions we also calculated the CME gravitational potential energies $E_{\rm pot}$ at the times of the kinetic energy calculations.

To appreciate the differences between the current CME measurements and those used in previous works, we have compared the 37 CMEs common to our 120 events with those of Gopalswamy et al. (2004, 2005c) from the CDAW catalog. The top panel of Figure 2 compares the 32 kinetic energies $E_{\rm kin}$(cdaw) taken or computed from the tables of Gopalswamy et al. (2004, 2005c; five CMEs had no mass determinations) with $E_{\rm kin}$(fr) calculated from our V(fr) speeds and CME masses. The $E_{\rm kin}$(cdaw) are a factor ∼1.4 larger than $E_{\rm kin}$(fr).

The 37 V(fr) and V(cdaw) speeds correlate well at CC = 0.93, with the average 1588 km s^{-1} V(fr) speed slightly higher than the 1569 km s^{-1} V(cdaw). Thus both our V(fr) and $E_{\rm kin}$ (fr) values match well with the previously determined CDAW counterparts used in the Mewaldt et al. (2008) analyses. Although somewhat redundant, we will continue our CME–SEP event comparisons using both the V(cdaw) and V(fr) values.

Another basic comparison is that of the V(cm) with the V(fr) speeds. Figure 2 (bottom) shows the comparison, which involves

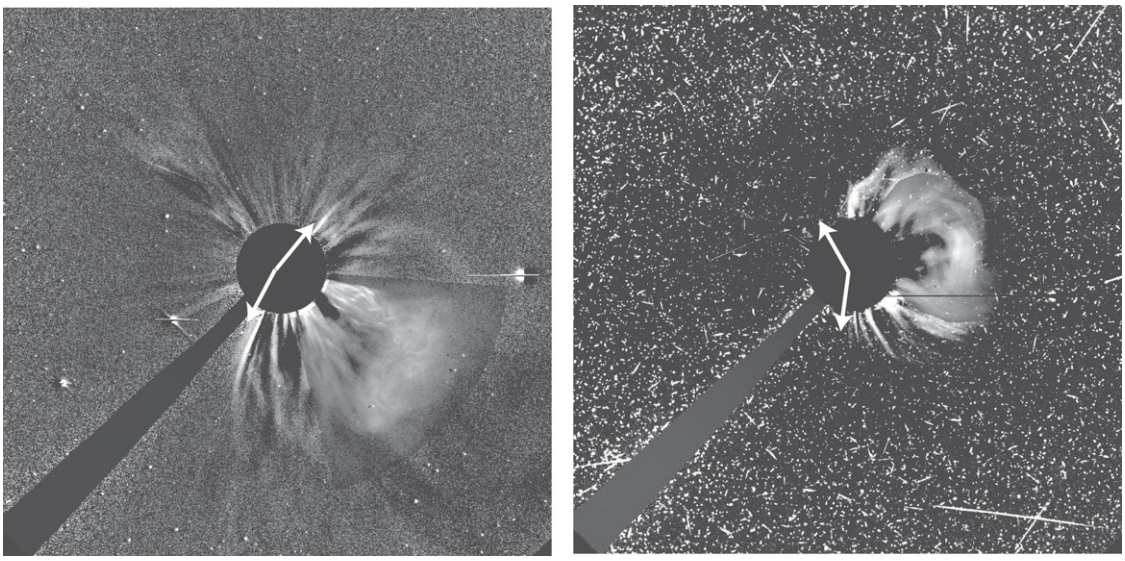

Figure 1. Examples of our mass measuring methodology. Left: excess-mass LASCO/C3 image on 2000 May 4 at 13:42 UT. The sector used for the mass measurement is shown with a contrast different from the rest of the images. Right: excess-mass LASCO/C3 images on 2001 December 26 at 6:42 UT. The mass was measured within a hand-drawn region-of-interest (ROI) made visible by the lower contrast. The effect of the enhanced cosmic ray background was removed by subtracting the average mass of a similar ROI over an area devoid of a CME. The arrows in both images mark the width reported in the CDAW catalog which usually includes the shock and deflected streamers and hence overestimates the mass.

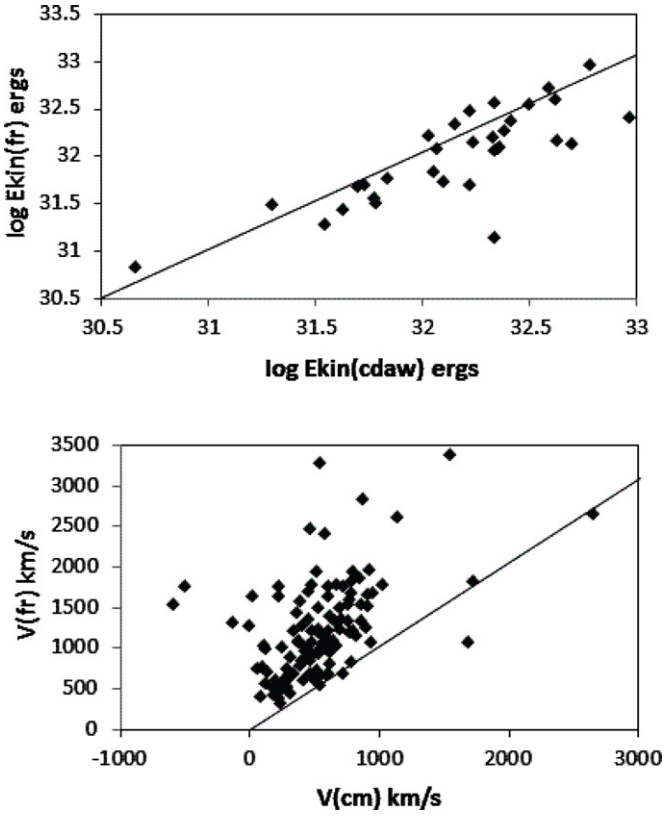

Figure 2. Top: comparisons of E_{kin}(fr) with those of Gopalswamy et al. (2004, 2005c). Leading-edge CME speeds were used for the calculations. Bottom: a direct comparison of the 120 frontal CME speeds V(fr) and V(cm). Note that some V(cm) values are negative and several are larger than the matching V(fr). Diagonal lines indicate equality in both plots.

several negative V(cm) values. Perhaps the best comparison is with median values, for which that of V(cm), 522 km s^{-1}, is less than half of the 1072 km s^{-1} V(fr) value. And, as expected, the E_{kin} (cm) were almost always less than E_{kin} (fr), as discussed in detail below.

2.2. The SEP Fluence Calculations

2.2.1. Previous SEP Fluence Calculations

The calculation of the total energy transferred from a CME into SEPs involves a comparison of the CME, remotely imaged in its entirety, with a temporally and spatially varying distribution of SEPs sampled only locally in situ at 1 AU. The primary challenge here is the estimation of the SEP event energy over its full energy range and duration, i.e., the fluence. In their study of the large 2002 April 21 SEP event Emslie et al. (2004) obtained fluence spectra over a four day period of the most abundant elements in the energy range from ~0.1 to 100 MeV nuc^{-1}. They extrapolated the energy spectra to lower and higher values and converted the intensity measurements to particles per cm^2 at 1 AU. Multiple crossings of individual particles at 1 AU due to scattering were considered, and they assumed a longitudinal and latitudinal spatial distribution to arrive at the SEP energy estimate, considered accurate to within a factor of four. Mewaldt et al. (2005a) treated their five SEP events in a similar fashion, and they found that 98% of the energy content was included in the range 0.1–100 MeV nuc^{-1}. Electrons constituted from ~1% to ~18% and protons 65% to 82% of the event total energies. With their additional 11 SEP events, Mewaldt et al. (2005b) assumed that the protons made up 75% of the total particle energy.

In their last SEP–CME energetics study of 23 events Mewaldt et al. (2008) made separate corrections for multiple particle crossings at 1 AU and for adiabatic energy losses. In a subsequent simulation Chollet et al. (2010) found that the two effects essentially balanced each other, so that SEP energy estimates from 1 AU measurements were insensitive to the combination of the two effects.

2.2.2. Fluence Estimates of the SEP Events from the EPACT Data

For the SEP events of our study we have both 2 MeV and 20 MeV proton differential intensity profiles from the *Wind*/EPACT instrument. The events were first selected on the basis of a 20 MeV intensity increase of at least a factor of two above background that could be confidently associated with

a fast CME (Kahler 2013). The intensity–time profile of each 20 MeV SEP event was characterized by a rise time T_R from onset to one-half the peak intensity Ip20, and a duration time T_D over which the intensity was within one-half Ip20. The 20 MeV proton intensity profiles were usually accompanied by 2 MeV proton and 2 MeV nuc^{-1} He intensity profiles time delayed by velocity dispersion. We have estimated a duration time T_D for each 2 MeV intensity event profile, taking into account the intrinsically higher levels of fluctuations in that energy band compared with those in the 20 MeV intensities. In 24 of the 120 events the 2 MeV proton increases above background were judged too poorly defined to determine 2 MeV event fluences, usually due to background fluctuations large compared to the 2 MeV intensity increases. Thus for 96 events we determined two-point power-law spectral exponents γ and H/He at 2 MeV nuc^{-1} and refer to these as spectral events. We could not determine T_D for one additional event, so the fluence calculations were based only on the remaining 95 SEP events. The median T_D for the 2 and 20 MeV events were 20 and 12.5 hr, respectively, and our assumed SEP event duration was taken as the arithmetic mean of the 2 and 20 MeV T_D values. The fluence F for each event is then taken as the peak energy spectrum times the averaged T_D.

To determine a peak proton energy event spectrum from 0.1 to 100 MeV, we extrapolated to those limiting values from an assumed power-law energy spectral fit based on the peak 2 and 20 MeV energy intensities Ip2 and Ip20. The extrapolation is only a factor of five in energy at the high energy end, but 20 at the low end. The spectra of five large SEP event fluences shown in Mewaldt et al. (2005a) suggest that our extrapolations likely overestimate the SEP intensities slightly in the 0.1 MeV $< E <$ 1 MeV range and more seriously in the $E >$ 50 MeV range, where the steeper spectra are better fit with double power-law or similar fits. We have recalculated the event energies with 60 MeV rather than 100 MeV cutoffs and find that the reductions exceed 20% for only 12 of the 96 events. Only the outward-propagating SEPs are considered here, so we multiply the differential angular intensities by a solid angle of 2π, a factor two less than the 4π used by Mewaldt et al. (2008).

Following the earlier Mewaldt et al. (2008) results, we further assume for our SEP energy estimates: (1) the proton spectrum alone yields all of the total SEP energy, (2) all the energy is included in the 0.1–100 MeV nuc^{-1} range, and (3) no SEP multiple-crossing or adiabatic-loss corrections are needed. We estimate the uncertainties of the SEP energy estimates as factors of ∼3. A strength of this analysis is that all the SEP measurements come from a single instrument and are uniformly treated in the analysis.

A systematic problem with the SEP event energies not treated here is the statistical hardening of the energy power-law spectral index γ with increasing solar source longitude. This has been found for many events in the 20–40 MeV (Cane et al. 1988) and in the $E >$ 10 MeV (Kahler 2001) energy ranges. In our 96 SEP events there is a weak correlation coefficient CC = −0.17 between spectral index γ and solar longitude, with about a 10% significance level (Bevington & Robinson 2003). The average value of γ for our SEP events decreases from ∼2.7 to 2.3 from W40° to W100°. This suggests that the lower energy ranges of the spectra of some far western SEP events are underestimated.

2.3. Esep: Estimates of the SEP Spatial Distributions

The final factor in the calculation of Esep is the assumed angular spatial distribution of the event. Based on a plot of peak intensities of NOAA SEP events versus solar source longitudes that showed a peak at central meridian, Emslie et al. (2004) and Mewaldt et al. (2005b, 2005c) assumed an e-folding intensity decrease of 25° for eastern and 45° for western hemisphere events. This is similar to the 25° e-folding decrease used in the empirically based SEP intensity-time model of Smart & Shea (1992), although their peak SEP intensities at 1 AU were assumed to be located at the magnetic connection to the flare longitude and maximized for flares or CMEs located at ∼W40°–W70°.

Multiple spacecraft observations of individual events are a better way to deduce spatial gradients, and Lario et al. (2006) used *Helios* and IMP-8 4–13 and 27–37 MeV events to deduce the best e-folding fits of 62° for events within 40° of the peak longitude, but only 12° for more distant (>40°) events. Their best-fit peak longitudes were shifted ∼16° and ∼26° east of the solar source longitudes for the 27–37 MeV and 4–13 MeV proton intensities, respectively. The eastward displacements of SEP event peaks from magnetic connections to flare/CME source longitudes increase with decreasing energies, as argued by Lario et al. (2006) and found observationally by Smart & Shea (1995).

We assume here that the latitudinal and longitudinal SEP intensity distribution at 1 AU is described by a simple rotationally symmetric exponential function with a 45° e-folding width. Since our energy spectrum is based on 2 and 20 MeV proton intensities, we center the distribution on a peak longitude displaced 26° eastward from the CME source region to match the Lario et al. (2006) result. That distribution is integrated over the full 1 AU sphere and yields the following result for the total SEP kinetic energy Esep in erg:

$$\text{Esep} = 5.46 \times 10^{24} \times F \times \exp((\theta_0 - 26^\circ)/45^\circ),$$

where F is the event fluence and θ_0 is the solar longitude of the CME source region in degrees west of central meridian. For all events over the west limb we used $\theta_0 = 110^\circ$. All the selected source regions lie west of W40°, so the neglect of latitudinal displacements should result in only slight underestimates of the observer separations and the resultant Esep. We may compensate by our use of a broader latitudinal e-folding width than that used by Mewaldt et al. (2008) (45° versus 25°).

For their 20 SEP events Emslie et al. (2012) used the Gaussian spatial distribution preferred by Lario et al. (2006), rather than the exponential form we used. The Gaussian form gives a flatter distribution near the peak of the event, but drops more steeply at the flanks. Emslie et al. (2012) found the Gaussian to produce a slightly lower Esep by a mean difference of only 16% from the exponential form (Mewaldt et al. 2008). Note that we truncate the integration after only two e-folding distances (90°) from the peak, so the differences between the two assumed spatial distributions should be only a second order effect here.

3. RESULTS

Each of the 120 SEP events is characterized by the 20 MeV peak intensity Ip20. For the 96 spectral SEP events we have three SEP parameters: the total SEP energy Esep (95 events only), the energy spectral index γ, and the H/He ratio at 2 MeV nuc^{-1}. Each of the corresponding CMEs is characterized by its mass M and its gravitational potential $E_{\rm pot}$, measured at the time of observed peak mass when $E_{\rm kin}$ is determined. The other CME parameters are the pairs of speeds V(fr) and V(cm) and the corresponding kinetic energies determined from

Table 1
Correlation Coefficients[a] between the SEP Event and CME Parameters

SEP/ CME	Log Ip20	Log Ip2	2–20 MeV Spectral $-\gamma$	Log SEP Event Energy	Log H/He 2 MeV nuc^{-1}
(1) V(cdaw)	0.61	0.58	0.19	0.48	−0.32
(2) V(cm)	0.36	0.41	0.00	0.34	−0.28
(3) V(fr)	0.59	0.58	0.16	0.50	−0.28
(4) log mass	0.37	0.37	0.19	0.36	0.11
(5) log $E_{\rm kin}$(fr)	0.59	0.59	0.18	0.56	−0.16
(6) log $E_{\rm kin}$(cm)	0.46	0.53	0.05	0.47	−0.17
(7) log $E_{\rm kin}$(fr) − log $E_{\rm pot}$	0.58	0.59	0.14	0.53	−0.31
(8) log $E_{\rm kin}$(cm) − log $E_{\rm pot}$	0.39[b]	0.47[c]	0.03[c]	0.39[d]	−0.22[c]
(9) log ($E_{\rm kin}$(fr) + $E_{\rm pot}$)	0.59	0.58	0.20	0.54	−0.13
(10) log ($E_{\rm kin}$(cm) + $E_{\rm pot}$)	0.53	0.55	0.16	0.49	−0.10

Notes.
[a] A 1% statistical significance of correlation requires a CC $\geqslant$ 0.23 for the 120 SEP events with logs Ip20 in Column 2 and a CC $\geqslant$ 0.26 for the 96 SEP events with parameters in Columns 3, 4 and 6 and the 95 SEP events of Column 5.
[b] Values calculated for 119 events, excluding 1 outlier with small log $E_{\rm kin}$(cm) − $E_{\rm pot}$.
[c] Values calculated for 95 events, excluding 1 outlier with small log $E_{\rm kin}$(cm) − $E_{\rm pot}$.
[d] Values calculated for 94 events, excluding 1 outlier with small log $E_{\rm kin}$(cm) − $E_{\rm pot}$.

those speeds, $E_{\rm kin}$ (fr) and $E_{\rm kin}$ (cm). With the goal of seeking physical insights and/or space weather forecasting tools, we carry out correlations between each of the various SEP event and CME parameters. The large dynamic range of most parameters requires us to do the correlations with logs of some parameters. The basic numbers for assessing our comparisons are that 5% or 1% statistical significance levels for the 120 events require correlation coefficients of CC = 0.18 and 0.23, respectively (Bevington & Robinson 2003). For the 96 spectral SEP events the corresponding requirements rise to CC = 0.20 and 0.26, respectively. Since the primary goal is to determine how SEP parameters depend on CME characteristics, we organize this analysis section in terms of the independent CME parameters. Our CCs are presented in Table 1.

3.1. CME Speeds

As a basis for comparison with the earlier SEP event studies (Kahler 2001), we first look at the correlation of the logs of the SEP peak intensities Ip20 and Ip2 with the leading-edge CME speeds V(cdaw) given in the LASCO CDAW catalog and with the CME frontal speeds V(fr) of the current analysis. As discussed above, V(cdaw) and V(fr) are well correlated with each other. Since the range of CME speeds is less than a decade, we prefer to use the linear speed values in our correlations. The logs of Ip20 are significantly correlated with V(cdaw) and V(fr) at CC = 0.61 and 0.59 for the full 120 SEP events (Figure 3). CC = 0.36, much lower, however, for the 120 SEP events with V(cm) (Figure 3, lower panel). To match more closely the plots of Kahler (2001) and Gopalswamy et al. (2003, 2004), we have replotted the V(cdaw) and V(fr) plots of Figure 3 in a log V format. The CCs decline slightly to CC = 0.56 for each log V plot, and we get fits of Ip20 $\sim V^{3.4}$, similar to our estimate of the slope of the fit of 21 frontside $E > 10$ MeV proton events of Gopalswamy et al. (2004), but not so steep as the $\sim V^{4.8}$ fit of 20 MeV proton events of Kahler (2001).

The SEP energy spectral index $-\gamma$ was uncorrelated with all three CME speed parameters. This might imply that the SEP Ip2 are poorly correlated with CME speeds, but we find that the logs of the 96 Ip2 peak intensities correlate with the V(cdaw) and V(fr) speeds with robust CCs of 0.58, only slightly less than for the logs of the Ip20. Thus, the fact that both SEP energy peaks Ip2 and Ip20 are well correlated with at least the V(cdaw) speeds does not preclude the large range of variation in γ, for which the standard deviation is 0.79 for the 96 SEP events.

Logs of both Esep and H/He correlate with all three CME speeds and are reported in Table 1. The correlation of Esep with V(cm) is lower than with V(fr) as one might expect if the frontal speed is the dominant factor in producing the SEP-accelerating shocks. The correlations of the logs of H/He, shown in Figure 4, are somewhat surprising, first for being negative. One possibility is that in the fastest CMEs the high SEP intensities may reach streaming limits (Reames & Ng 2010), resulting in depressed intensities of protons relative to the higher rigidity He particles. If that were the case, we might expect logs of H/He to correlate inversely with logs of Ip2 or Ip20, but those parameters correlate at only CC = −0.11 and −0.04. We also find no correlation (CC = 0.07) between logs of H/He and the corresponding $-\gamma$. The large correlation here is CC = −0.49 between the logs of H/He and 2 MeV nuc^{-1} He peak intensities, significant at <0.1%. This indicates that the He abundances vary essentially independently of either Ip2 or Ip20. It is further surprising that the negative correlations of logs of H/He with logs of V(cm) and of V(fr) should be comparable, when the SEP energetic correlations are generally lower for V(cm) than for V(fr). This may be a coincidence, or it may provide a clue to the general relationship between H/He and CME speeds.

3.2. CME Masses

The fourth line of Table 1 gives the correlations of the SEP parameters with CME masses. We find that the logs of Ip20 and of total energy Esep are correlated with the logs of the CME masses, with CC = 0.37 and 0.36, respectively, as shown in Figure 5.

There is a weak but not significant (CC = 0.19) trend for the spectral index $-\gamma$ to get harder (increase) with increasing mass. We previously found (Section 2.2.2) that γ decreases with increasing longitude, and we also find that log M increases slightly with longitude by 0.18, or a factor of 1.52, from W40° to W100°. Thus we attribute the weak correlation of $-\gamma$ with log M to the fact that both parameters share a common

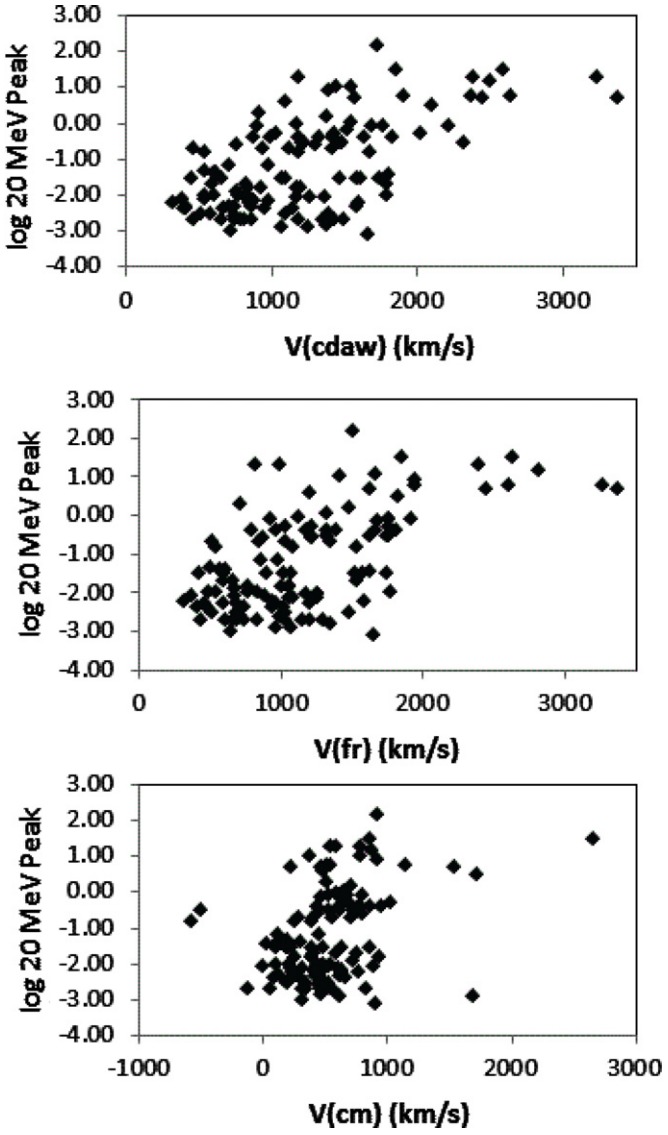

Figure 3. Logs of the peak 20 MeV proton intensities vs. three sets of CME speeds. Top: the V(cdaw) speeds of the LASCO catalog. Middle: the CME speeds determined for the CME fronts. Bottom: the CME speeds for the centers of mass, three of which are negative. The correlations are significant in all plots.

weak longitudinal dependence which is expected to produce the observed trend for harder spectra with increasing mass. The H/He ratio versus CME mass correlation, at CC = 0.11, is not significant.

3.3. CME Energies

3.3.1. Kinetic Energies

As discussed earlier, the CME kinetic energies $E_{\rm kin}$ (fr) are calculated on the basis of the frontal speeds V(fr), which implicitly assumes that all the CME mass is moving at that speed, and $E_{\rm kin}$ (cm) by integrating over the kinetic energies of all the individual CME mass elements. The median log of $E_{\rm kin}$ (fr) in erg exceeds that of the log $E_{\rm kin}$ (cm), which we take as a more realistic CME energy evaluation, by 31.57–30.91, or a factor of ∼4.4, for the 120 CMEs.

The CCs for all the CME kinetic energy and SEP event parameter comparisons are given in lines 5 and 6 of Table 1. Only the Ip20, Ip2, and Esep parameters reach the 1% CC significance level, and that is the case with both the $E_{\rm kin}$ (cm) and

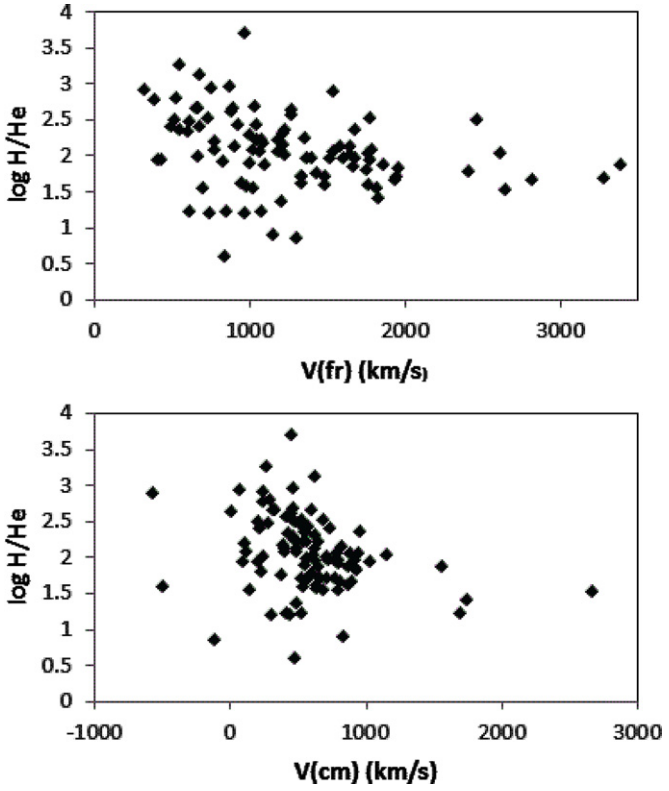

Figure 4. Correlation of the 96 H/He ratios at 2 MeV nuc^{-1} with the V(fr) (top) and V(cm) (bottom) CME speeds.

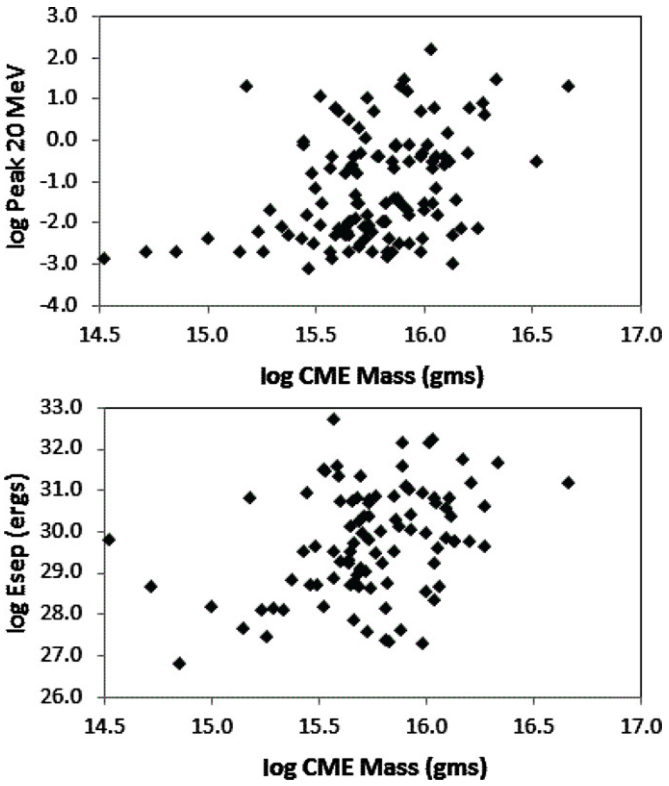

Figure 5. Top: plot of the correlation (CC = 0.37) of logs of Ip20 vs. logs of CME masses for 120 SEP events. Bottom: plot of the correlation (CC = 0.36) of the logs of Esep vs. CME masses for 95 spectral SEP events.

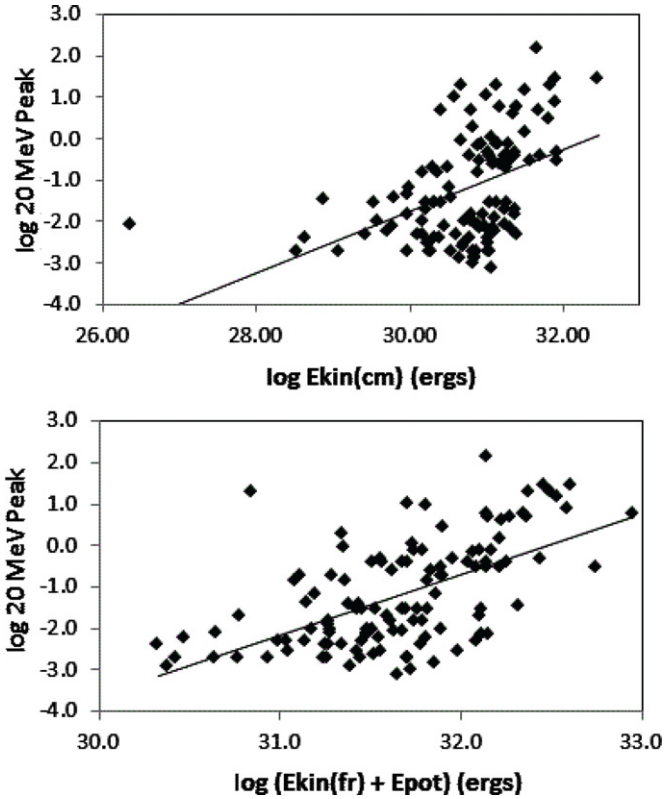

Figure 6. Top: plot of 120 logs of Ip20 vs. logs of E_{kin} (cm) in erg. The slope of the least-squares best fit line is 0.75. Bottom: similar plot of logs of Ip20 vs. logs of (E_{kin} (fr) + E_{pot}), both in erg. The slope of the best fit is 1.46.

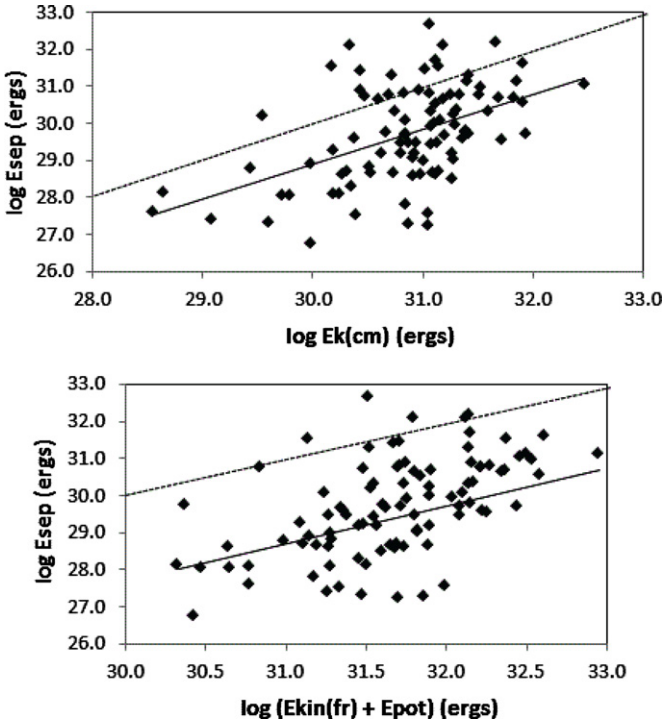

Figure 7. Top: plot of logs of Esep vs. the logs of the E_{kin} (cm) for 94 spectral events. One outlier with log E_{kin} (cm) = 26.4 is deleted. Bottom: plot of the logs of Esep vs. the logs of (E_{kin} (fr) + E_{pot}) for 95 spectral events. Top dashed line of each plot follows equality of the two energies. Solid lines are least-squares best fits with slopes of 0.94 (top) and 1.33 (bottom).

E_{kin} (fr) CME energies. Those correlations are clearly higher for E_{kin} (fr) than for E_{kin} (cm). For Ip20 the E_{kin} (cm) correlation, shown in the top of Figure 6, is lower than that of E_{kin} (fr), a result similar to the lower V (cm) correlations of Figure 3. These results indicate that CME leading-edge speeds provide a better match than center of mass speeds for SEP production.

The comparisons of Esep with the CME kinetic energies are of interest not only for their correlations but also for a comparison of the absolute energies as a measure of the efficiency of conversion of CME energy into Esep. The top of Figure 7 shows the plot of Esep versus E_{kin} (cm), the smaller of the calculated CME energy parameters. Fourteen points lie above the equality line, indicating that Esep exceeds E_{kin} (cm). The best-fit line slope is 0.94 when the log E_{kin} (cm) outlier at 26.37 on the left side is deleted. For the generally larger logs of E_{kin} (fr), only five points exceed the equality line and the slope is 1.19. These results point to high ratios of SEP to CME energies as well as a consistency with a linear relationship.

3.3.2. Combining Kinetic and Potential Energies

In this section we strive for more realistic CME energy estimates by including the gravitational potential energies E_{pot}, each measured at the same time as that of the corresponding CME kinetic energy E_{kin} (cm) or E_{kin} (fr). The potential energy is a large fraction of the total CME energy budget. The median log of the CME potential energies E_{pot} is 30.95, comparable to the 30.99 median for the logs of E_{kin} (cm), but less than the 31.60 median for the logs of E_{kin} (fr). The addition of the potential to the kinetic energies means statistically that the largest calculated CME energies will be those of E_{kin} (fr) + E_{pot} given in line 9 of Table 1.

One can take several approaches to the inclusion of the parameter E_{pot}. By adding it to the E_{kin} (cm) and E_{kin} (fr) parameters, we get better representations of the total energies of the CMEs as observed in the Sun-centered coordinate frame. On the other hand, E_{pot} is a measure of the CME energy expended to work against solar gravity and not available as a free energy for driving shocks. For a CME at a given coronal height and speed, the mass contributes roughly equally to the potential and the kinetic energies. If the CME potential energy is increasing at the expense of the kinetic energy, which is the source of the shock and SEP energies, then we might expect that SEP production would increase with an increase of E_{kin}/E_{pot}, or with log E_{kin} − log E_{pot}. If the CME kinetic energy is maintained or increased, perhaps by conversion of magnetic energy, then the SEP correlations with CME energies may be worse with the addition or subtraction of E_{pot}. By comparing SEP parameters with both the sums and the differences of the logs of E_{kin} and E_{pot}, we can look for an indication of whether the potential energies are relevant for the shock and SEP production. The correlations of SEP parameters with the energy differences and sums are given in lines 7–8 and 9–10 of Table 1. In doing the correlations for E_{kin} (cm) − E_{pot}, we omitted an outlier from 1997 October 7, which had a V (cm) of only 4 km s^{-1} and a very small E_{kin} (cm). That outlier is obvious in the top panel of Figure 6.

We note first that Ip2, Ip20, and Esep correlate with all six CME energy parameters. The Ip20 correlations with E_{kin} (fr) and (E_{kin} (fr) + E_{pot}) are comparable to those with V (fr). In Figure 6 we compare poor (top, E_{kin} (cm)) and good (bottom, (E_{kin} (fr) + E_{pot}) correlations of the Ip20 parameter. The relatively flat slope of 0.75 for E_{kin} (cm) is obviously skewed by several outliers; the slopes are larger than unity for the other Ip20

correlations, implying possibly greater than linear increases in Ip20 with CME kinetic energy.

Correlations of log Esep with various forms of CME energies for the 95 spectral events are also all significant and comparable to each other. [log E_{kin} (cm) − log E_{pot}] has the lowest median values of all the CME energy parameters and is plagued by small-value outliers, reducing the CC. The log Esep versus the log E_{kin} (cm) plot is shown in comparison with that of (E_{kin} (fr) + E_{pot}) in Figure 7. The 0.94 and 1.33 slopes of those plots are consistent with linear correlations. The statistically largest of our CME energy parameters is that of (E_{kin} (fr) + E_{pot}) of Figure 7 (bottom), which provides the most conservative comparison of Esep with a CME energy. All points but five are now under the line of equality where Esep = (E_{kin} (fr) + E_{pot}), in contrast to the 14 points of the plot of E_{kin} (cm) in Figure 7 (top). If E_{kin} must always exceed Esep, then at least E_{kin} (cm) is a substantial underestimate of the true CME energy. It may better measure the internal dynamics of CMEs, in contrast to the more global kinematics of E_{kin} (fr). In this view E_{kin} (cm) and E_{kin} (fr) would be lower and upper limits to an optimum value of E_{kin}. E_{kin} (cm) is also the only parameter for which the log–log plot slope is less than unity. The results of the Ip20 and Esep plot comparisons suggest that Ip20 but not Esep increases faster than linearly with the CME energies.

In general there is little difference among the SEP parameter correlations with the different CME energy parameters. The main reason for this result is the fact that E_{pot} itself is also correlated with the SEP parameters of Table 1 at values close to those of the log mass correlations of line 4 of Table 1. Since both E_{pot} and E_{kin} are proportional to CME masses, these results again point to the important role of the CME masses for SEP production.

3.3.3. The Power-law Spectrum and H/He Ratio Comparisons

The SEP event parameter $-\gamma$ generally shows slightly positive (i.e., harder) trends with increases of each of the various CME energy parameters, as shown in the positive CCs of lines 5 through 10 of Table 1. As an illustration of the small trend and high degree of scatter of the $-\gamma$ comparisons, we show the comparison with E_{kin} (fr) in the top panel of Figure 8.

Although we earlier found significant correlations of H/He with CME speeds, the H/He ratios show consistent but not significant negative correlations with the various CME energy parameters. Only one combination, that of H/He versus log E_{kin} (fr) − log E_{pot} rises to the 1% significance level at CC = −0.31, and that plot is shown in the bottom panel of Figure 8.

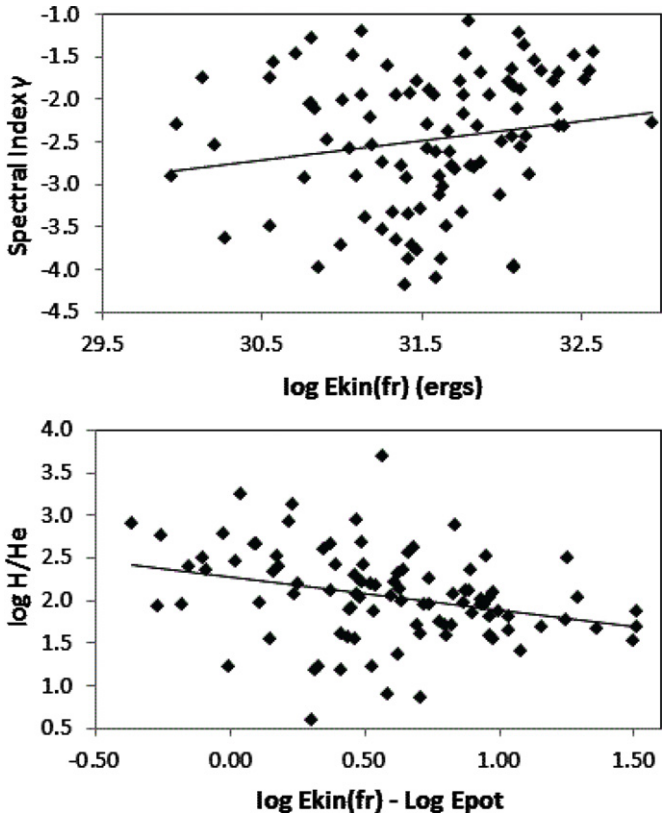

Figure 8. Top: plot of spectral index γ vs. the logs of the E_{kin} (fr) for the 96 spectral events. None of the correlations of γ is significant, although all show slight positive trends. Bottom: plot of the logs of 2 MeV nuc^{-1} H/He vs. log E_{kin} (fr) − log E_{pot}. This is the only significant correlation between H/He and a CME energy parameter. Solid lines are least-squares best-fit slopes.

4. DISCUSSION

4.1. Limitations to the Analysis

4.1.1. SEP Propagation and Longitude Effects

To calculate the total SEP energies Esep, it was necessary to make a number of simplifying assumptions, as discussed in Section 2. Perhaps the most uncertain factor is that of the SEP spatial distributions. Mewaldt et al. (2005b, 2005c) and Lario et al. (2006) have used peak SEP intensities measured at different longitudes or on different spacecraft to infer characteristic exponential or Gaussian distributions. However, the spatial widths of the SEP events may be highly variable from event to event. Exceptional SEP events originating from the near central meridian of the backside of the Sun have long been noticed (Dodson et al. 1969; Cliver et al. 2005; Miyasaka et al. 2005; Dresing et al. 2012) and a number of SEP events extending to 300° in longitude have been discussed (Cane 1995; Cliver et al. 1995). These broad SEP distributions have been interpreted in terms of SEP injections following the coronal azimuthal propagation of CME-driven shocks across field lines connected to the interplanetary observer (Cane 1995; Cliver et al. 1995, 2005; Rouillard et al. 2011, 2012). Thus the angular extents of large SEP events may considerably exceed the narrower approximations used here, resulting in underestimates of Esep values.

Two other considerations, however, suggest overestimations of Esep. The first is that SEPs may propagate into closed magnetic field structures that result in confinements and intensities enhanced above those expected from the open field propagation models of Chollet et al. (2010) or Li et al. (2003). Comparing the two SEP events of 2002 April 21 and August 24, with similar flare and CME source associations, Tylka et al. (2005) interpreted the longer high-energy SEP duration of the April 21 event in terms of quasi-parallel, rather than quasi-perpendicular, shock acceleration. However, Tan et al. (2008, 2009) showed that the longer duration event resulted from the presence of a reflecting boundary inside a magnetic cloud, whereas the shorter duration August 24 event was characterized by a free streaming of the SEPs.

The second consideration is that most gradual SEP events undergo a decay phase characterized by a confinement of the SEPs in a spatial region behind the shock known as a reservoir. Thus integrating the duration of the SEP intensity through the reservoir can erroneously count as freely propagating and relatively newly accelerated those particles which have been

trapped for many hours in the reservoir (Reames et al. 2013). The 20 MeV SEP durations here extend only to the time of the shock if the intensities are still more than half the peak intensities Ip20. Our estimates of Esep undoubtedly suffer from the assumption of a common spatial distribution for all SEP events, but we expect that this uniform treatment of all events will allow us to bring out basic trends in the CME–SEP event relationships.

4.1.2. CME Thermal Energies

The coronagraph observations of Thomson-scattered light yield CME masses and mass motions and heights but do not allow us to determine either the magnetic or the thermal energies of CMEs (Murphy et al. 2011). These quantities must be estimated from other sources. In an analysis combining *Hinode*, *STEREO-A*, and *SOHO* EUV observations, Landi et al. (2010) found that the thermal heating of a 2008 April 9 CME exceeded its kinetic energy. More generally, Murphy et al. (2011) have reviewed four different lines of observational evidence to show that the thermal energy input into CMEs is comparable to the kinetic energy (thus confirming the earlier results of Akmal et al. 2001). They then analyzed six features composing the 2000 June 28 CME and found heating energies comparable to or greater than the kinetic energies of four features. Although these results are obtained at relatively low heights ($<4\ R_\odot$), they show that the thermal energies may be an important factor in the CME energy budgets that are not captured in this analysis.

4.1.3. CME Magnetic Energies

All models of CMEs assume that the eruptive energies are powered by the conversion of the magnetic field energy contained in magnetic flux tubes (Jacobs & Poedts 2011). Although a large fraction of the magnetic energies are converted into other forms of energy during the eruptions, the magnetic energies may be important components of CME energy budgets. These energies can only be estimated on the basis of models or of interplanetary CME in situ field observations. In the Chen (1996) model of an energetic CME with an injection of $\sim 10^{32}$ erg of poloidal field energy to drive the propulsion, the initial toroidal energy remained essentially unchanged at $\sim 10^{31}$ erg, roughly two or three times less than the CME kinetic energy. On the other hand, Wu et al. (1997) applied a flux rope model to observations of a large CME observed by LASCO and calculated a magnetic energy of $\sim 4 \times 10^{31}$ erg, comparable to the potential energy but an order of magnitude more than the kinetic energy. Vourlidas et al. (2000) compared CME energies from LASCO observations to estimate the magnetic energies based on averages of magnetic cloud observations at Earth and assuming magnetic flux conservation. They found for the fastest cases that the magnetic energies were significantly below the potential and kinetic energies. However, for a set of 39 flux-rope CMEs Subramanian & Vourlidas (2007) found that the internal magnetic fields were sufficiently large to be viable sources of the continued driving power in the 2–20 $R_\odot$ range. We cannot determine the magnetic energy contributions on the basis of the CME observations, but it seems likely that excluding that energy component implies larger CME energies than we have estimated here.

4.1.4. CMEs in the Solar Wind (SW) Frame

In this work we calculated the CME speeds and energies in a Sun-fixed coordinate system. An alternative method is to use a CME coordinate system tied to the SW on the assumption that SEP acceleration can occur only when a CME is moving sufficiently fast in the SW frame to drive a shock (Mewaldt et al. 2008). This may be a reasonable assumption when the CME-SW geometry approximates the one-dimensional geometry of a piston driving a parallel shock. However, earlier observations (Cane 1995; Cliver et al. 1995, 2005) suggested a close connection of SEP acceleration and injection with the azimuthal coronal propagation of shock waves, an idea now supported by observations of the well-studied EUV waves driven at least initially by the expanding flanks of fast CMEs (Rouillard et al. 2011, 2012; Démoulin et al. 2012; Patsourakos & Vourlidas 2012). These coronal shock waves are at least initially quasi-perpendicular and may bear little resemblance to the quasi-parallel shocks arising later in the SW ahead of the radially expanding shock. Even then, the distortion and draping of field lines by the CME (Das et al. 2011) may considerably alter the simple concept of the piston-driven parallel shock.

The median values of V(fr) and V(cm) for our 120 events are 1072 km s^{-1} and 522 km s^{-1}, respectively. Subtracting a SW speed of 400 km s^{-1} from these CME measured speeds reduces those speeds by 37% and 77% and the $E_{\rm kin}$ (fr) and $E_{\rm kin}$ (cm) energies even more, by 61% and 95%. The CME speeds and energies are thus significantly underestimated when the SW speed is subtracted in the calculation. The CME energies may also be seriously underestimated by omitting the energies of the coronal lateral expansions that drive the EUV waves, as estimated by Patsourakos & Vourlidas (2012), but this effect is likely important only during the early stages of CME formation. It should cease by 1–15 $R_\odot$ where we take our measurements.

4.2. Implications of Results

The basic goal of this work has been to compare statistically properties of gradual SEP events with those of the associated CMEs that drive the shocks producing the SEPs. We selected events from a restricted longitude range of $>$W40° to allow for a more homogeneous data set in terms of SEP propagation and CME azimuthal brightness variations. The expectation is that the large statistical base will allow us to uncover possible CME–SEP scalings in the presence of large systematic and random uncertainties in the calculations of these parameters.

It is still necessary to make rather sweeping assumptions of the unobservable properties of both the spatial and temporal variations of the SEP production and of the intrinsic properties of the CMEs, as detailed above. By careful integration of the CME outlines we are able to get more realistic determinations of the CME potential and kinetic energies than has been done before (Mewaldt et al. 2008). The large dynamic range of the selected ~20 MeV SEP events enables us to look for parametric CME–SEP scalings difficult to discern with only large SEP events. However, for 24 of the 120 SEP events with small peak intensities or high backgrounds, it was judged not possible to determine the 2 MeV proton intensity profiles required for our spectral and total energy approximations.

The correlation of peak intensity Ip20 versus CME speed V(cdaw) (Kahler 2001) was an early line of evidence connecting the production of gradual SEP events to CME shocks. We confirm the correlation with the V(cdaw) and V(fr) speeds, although the CC of 0.60 is less than the previous value of CC = 0.72 for the combined plot of *Helios* and Solwind Ip20 data shown in Figure 1 of Kahler (2001). We find a lower but significant CC = 0.36 of Ip20 with V(cm), perhaps expected since it is the shock at the front of the CME that produces the

SEPs, and V(fr) is a better measure of the nose of the driven shock, inferred (Lario et al. 2006; Bemporad & Mancuso 2011; Reames et al. 2013) to be the source of peak SEP intensity. On the other hand, when we include the CME potential energies to get better definitions of the total CME energies, we find only a slightly lower CC for ($E_{\rm kin}$ (cm)+ $E_{\rm pot}$) than for ($E_{\rm kin}$ (fr)+ $E_{\rm pot}$) (Table 1).

The CME mass is an important factor for both parameters Ip20 (CC = 0.37) and Esep (CC = 0.36), shown in Figure 5. This first result supports our (Kahler & Vourlidas 2005) previous finding that SEP-rich events had significantly higher CME masses than did SEP-poor events. That analysis had the advantage of removing the CME speed bias from the comparison of the two groups of SEP events, but as discussed in Section 1, they determined the CME masses and mass densities per pixel (or square degree) in the range 3–6 $R_\odot$, where the masses are still increasing and not yet at their final values. As in that work, we believe that the likely source of this correlation is simply that the higher masses are associated with wider CMEs. We find support for this interpretation in our significant correlation (CC = 0.32) of the CME masses with their widths, some of which are 360° halo CMEs. Gopalswamy et al. (2005a) found a higher CME mass-width CC of 0.63 for a large sample of 4138 CMEs with widths <120°, which omitted the halo CMEs.

A primary goal of this work was to follow the work of Mewaldt et al. (2008) to relate the total SEP energies Esep to the total CME energies. Their work found that Esep could be a significant fraction of the CME energy, ranging from 0.1% to >10%. We have made crude approximations to determine Esep for 95 SEP events and done the comparison with several versions of the CME energies, which include only the kinetic and potential energies. Esep correlates comparably well with five of our six CME energy parameters (Table 1).

There are two basic questions to address here. The first is to determine the efficiency of conversion of CME energy, appropriately measured, into Esep. As we discussed in the previous section, the calculation of the appropriate CME energy is fraught with problems, both observational and conceptual. For this purpose we show two of the correlation plots in Figure 7, that of a statistically small CME energy parameter, $E_{\rm kin}$ (cm), and the largest, ($E_{\rm kin}$ (fr) + $E_{\rm pot}$). In the latter case we find five events above the line of energy equality and many more points in the 10%–100% efficiency range. Taking ($E_{\rm kin}$ (fr) + $E_{\rm pot}$) as a high estimate of CME energy, we still find the high conversion efficiencies that Mewaldt et al. (2008) found.

The second question is the scaling of the SEP and CME energies. In the plots of log Esep versus log CME energies we find best-fit slopes of 0.94, 1.19 and 1.33 for the CME energy parameters of $E_{\rm kin}$ (cm), $E_{\rm kin}$ (fr), and ($E_{\rm kin}$ (fr) + $E_{\rm pot}$) (Figure 7), respectively, consistent with a direct proportion between the Esep and CME energies. We have to bear in mind that the plot has resulted from an initial selection of SEP events with observed associated CMEs and that a selection based on the most energetic observed CMEs for such a comparison may yield very different results.

This result also raises again the question of how the CME energy should be calculated. If we want to compare the total CME energy to the free energy available from the solar source region, then all forms should be included. We discussed above the fact that the coronagraph white-light observations yield the required kinetic and potential energies, but do not allow us to include either the plasma thermal energy or the magnetic field in the CME energy budget. Both kinds of energy are significant, so this presents a serious deficiency in the CME budget calculation. On the other hand, in our comparison with SEP event peak intensities and total energies, if we care only about the forms of energy available for driving the shocks that produce SEPs, then perhaps only the kinetic energy is relevant. This was the basis for the Mewaldt et al. (2008) assumption that the important calculation for SEPs should be the CME kinetic energy in the SW frame. We discussed above that that calculation implicitly assumes the formation of a quasi-parallel shock anti-sunward of the CME, which may not be the case, particularly for azimuthally expanding CMEs and shocks. We would further argue that the important factor relevant to the formation of a quasi-parallel shock is the CME speed, not the kinetic energy. The energy budget is further obscured by the possibility that adiabatic cooling of the thermal plasma and/or conversion of magnetic field energy could continuously enhance the kinetic energy of the evolving CME. To specify the conversion of coronal free energy into the CME energy and then into SEP energy would appear to require some detailed modeling to understand the full range of possibilities. The Esep plots of Figure 7 may provide guidance for such work.

We also looked for any correlations of SEP elemental abundances with CME properties, although our comparison was limited to the H/He ratios in the ~2 MeV nuc^{-1} range. SEP abundance variations are dependent on the seed populations and the shock geometry, as discussed by Tylka et al. (2005). If we find no correlations with CME properties, it may well mean that the seed population is the dominant factor in determining the relative SEP abundances. However, we do find significant correlations of decreasing values of H/He with each of the CME speed parameters (Figure 4), which suggests some role of the CME shock geometry for the SEP abundances. If we had found a much better correlation of H/He with V(cdaw) than with V(cm), as was the case for Ip20, then we might consider that parallel shocks, the most likely configuration at the leading edge, and near the central position angle of the CME to be most responsible. However, the CCs with V(cdaw) and V(cm) are comparable at −0.32 and −0.28, suggesting here that the expansion of the body of the CME is also playing an important role. This is consistent with recent observations relating EUV waves with delayed SEP onsets (Rouillard et al. 2011, 2012). In these SEP events it is the laterally expanding CMEs, driving quasi-perpendicular shocks, rather than the presumed quasi-parallel shocks at the CME leading edges, that seem to dominate the acceleration process of the observed SEPs. If H/He in the seed populations does not vary in SEP events, and the higher rigidity (M/Q = 2) He ions escape the shock more quickly than the lower rigidity (M/Q = 1) protons, then we might expect higher H/He in parallel shocks than in perpendicular shocks that can better retain the higher rigidity He ions for acceleration to reduce the 2 MeV nuc^{-1} H/He ratios. The distinction between parallel and perpendicular shock acceleration is better carried out with heavier ions and with energy spectral shapes (Tylka et al. 2005), which is beyond the scope of this work, but the CME speed dependence of the H/He ratio suggests a connection of CME speed to shock geometry.

5. SUMMARY

We have carried out a statistical comparison of the properties of 120 gradual SEP events with those of their associated CMEs. The events were chosen on the basis of observed SEP events, not on a CME-based selection criterion. SEP–CME solar sources of the events were limited to the longitude range >W40° to minimize variations in CME view angles and SEP

propagation. The CME masses, center of mass speeds V(cm), frontal speeds V(fr), and their derived kinetic energies $E_{\rm kin}$ (cm) and $E_{\rm kin}$ (fr) and potential energies $E_{\rm pot}$ were calculated as the CME parameters from *SOHO* LASCO observations. The SEP parameters were the 20 MeV peak intensities Ip20 observed with the *Wind* EPACT, and for a subset of 92 events with usable 2 MeV peak proton intensities Ip2, the power-law energy spectral index γ, the SEP event total energy Esep, and the 2 MeV nuc^{-1} H/He peak intensity ratios. We made crude but uniform approximations to calculate the peak SEP power-law energy spectra and the total event energies. Both the SEP peak intensities Ip20 and total energies Esep ranged over five orders of magnitude, but with substantial scatter such that the CCs of the logs of the parameters were generally $\leqslant$0.5. The goal was to search for statistical correlations that would provide insights into the physics of SEP production and allow possible CME signatures for space weather predictions of SEP events.

We first verified the previous (Kahler 2001; Gopalswamy et al. 2003, 2004) correlation of peak SEP intensities Ip20 with CME speeds. The leading-edge speed V(fr) appeared better correlated than V(cm), suggesting that SEP production is maximized at the fastest part of a given CME. Both the peak intensity Ip20 and the total SEP energy Esep correlate with the CME mass (Figure 5), a result consistent with enhanced SEP events resulting from broader CME angular extents. The correlation of CME masses with their angular widths supports this interpretation.

The correlations of Ip20 and Esep with CME energies were carried out for CME energies calculated both with the frontal and center of mass speeds and with and without adding the potential energies. Ip20 (Figure 6) and Esep (Figure 7) correlations were found for all six CME energy parameters. We confirm that Esep can range from $\leqslant$0.001% to $\sim$100% $E_{\rm kin}$ (cm), indicating that either the conversion from CME to SEP energy can be very high or the significant CME energy components are not included in the calculations.

The study included two other SEP variables, the estimated peak proton power-law spectrum derived from the peak 2 and 20 MeV proton intensities, and the 2 MeV nuc^{-1} H/He ratios. Overall, we found only a small but not significant tendency for spectral hardening (increasing $-\gamma$) with increasing CME masses and energies. The H/He ratio, which could reflect the seed population abundances or the physics of the shock geometry, was inversely correlated with all the CME speed parameters. If this result is associated with shock geometry, we suggest a scenario in which quasi-perpendicular shocks of faster CMEs contain the higher rigidity He ions at the shock fronts for enhanced acceleration. This could be the case if the faster CMEs also involve strong lateral expansions driving those shocks.

S.K. was funded by AFOSR Task 2301RDZ4. A.V. was supported by the NASA LWS TR&T program. We thank the reviewer for useful comments on the manuscript. CME data were taken from the CDAW LASCO catalog. This CME catalog is generated and maintained at the CDAW Data Center by NASA and The Catholic University of America in cooperation with the Naval Research Laboratory. *SOHO* is a project of international cooperation between ESA and NASA.

REFERENCES

Akmal, A., Raymond, J. C., Vourlidas, A., et al. 2001, ApJ, 553, 922
Balch, C. C. 1999, Radiat. Meas., 30, 231
Bemporad, A., & Mancuso, S. 2011, ApJL, 739, L64
Bevington, P. R., & Robinson, D. K. 2003, Data Reduction and Error Analysis (Boston, MA: McGraw-Hill)
Bothmer, V., & Zhukov, A. 2007, in Space Weather Physics and Effects, ed. V. Bothmer & I. A. Daglis (Chichester: Praxis), 31
Burkepile, J. T., Hundhausen, A. J., Stanger, A. L., St. Cyr, O. C., & Seiden, J. A. 2004, JGR, 109, A03103
Cane, H. V. 1995, in AIP Conf. Proc. 374, High Energy Solar Physics, ed. R. Ramaty et al. (Melville, NY: AIP), 124
Cane, H. V., Reames, D. V., & von Rosenvinge, T. T. 1988, JGR, 93, 9555
Carley, E. P., McAteer, R. T. J., & Gallagher, P. T. 2012, ApJ, 752, 36
Chen, J. 1996, JGR, 101, 27499
Chollet, E. E., Giacalone, J., & Mewaldt, R. A. 2010, JGR, 115, A06101
Cliver, E. W. 2009, in IAU Symp. 257, Universal Heliospheric Processes, ed. N. Gopalswamy & D. F. Webb (Cambridge: Cambridge Univ. Press), 401
Cliver, E. W., Kahler, S. W., Neidig, D. F., et al. 1995, in Proc. 24th Int. Cosmic Ray Conf. (Rome), 4, 257
Cliver, E. W., Thompson, B. J., Lawrence, G. R., et al. 2005, in Proc. 29th Int. Cosmic Ray Conf. (Pune), 1, 121
Colaninno, R. C., & Vourlidas, A. 2009, ApJ, 698, 852
Crosby, N. B. 2007, in Space Weather Physics and Effects, ed. V. Bothmer & I. A. Daglis (Chichester: Praxis), 131
Das, I., Opher, M., Evans, R., Loesch, C., & Gombosi, T. I. 2011, ApJ, 729, 112
Démoulin, P., Vourlidas, A., Pick, M., & Boutelle, A. 2012, ApJ, 750, 147
Dodson, H. W., Hedeman, E. R., Kahler, S. W., & Lin, R. P. 1969, SoPh, 6, 294
Dresing, N., Gómez-Herrero, Klassen, A., et al. 2012, SoPh, 281, 281
Emslie, A. G., Dennis, B. R., Holman, G. D., & Hudson, H. S. 2005, JGR, 110, A11103
Emslie, A. G., Dennis, B. R., Shih, A. Y., et al. 2012, ApJ, 759, 71
Emslie, A. G., Kucharek, H., Dennis, B. R., et al. 2004, JGR, 109, A10104
Gopalswamy, N. 2006, JApA, 27, 243
Gopalswamy, N., Aguilar-Rodriguez, E., Yashiro, S., et al. 2005a, JGR, 110, A12S07
Gopalswamy, N., Xie, H., Yashiro, S., & Usoskin, I. 2005b, in Proc. 29th Int. Cosmic Ray Conf. (Pune), 1, 169
Gopalswamy, N., Yashiro, S., Akiyama, S., et al. 2008a, AnGeo, 26, 3033
Gopalswamy, N., Yashiro, S., Krucker, S., Stenborg, G., & Howard, R. A. 2004, JGR, 109, A12105
Gopalswamy, N., Yashiro, S., Lara, A., et al. 2003, GeoRL, 30, 8013
Gopalswamy, N., Yashiro, S., Liu, Y., et al. 2005c, JGR, 110, A09S15
Gopalswamy, N., Yashiro, S., Xie, H., et al. 2008b, ApJ, 674, 560
Guetersloh, S., & Zapp, N. 2010, in Heliophysics: Space Storms and Radiation: Causes and Effects, ed. C. J. Schrijver & G. L. Siscoe (Cambridge: Cambridge Univ. Press), 359
Jacobs, C., & Poedts, S. 2011, JASTP, 73, 1148
Kahler, S. W. 2001, JGR, 106, 20947
Kahler, S. W. 2013, ApJ, in press
Kahler, S. W., Burkepile, J. T., & Reames, D. V. 1999, in Proc. 26th Int. Cosmic Ray Conf. (Utah), 6, 248
Kahler, S. W., Cliver, E. W., & Ling, A. G. 2007, JATP, 69, 43
Kahler, S. W., & Reames, D. V. 2003, ApJ, 584, 1063
Kahler, S. W., Reames, D. V., & Burkepile, J. T. 2000, in ASP Conf. Ser. 206, High Energy Solar Physics: Anticipating HESSI, ed. R. Ramaty & N. Mandzhavidze (San Francisco, CA: ASP), 468
Kahler, S. W., & Vourlidas, A. 2005, JGR, 110, A12S01
Landi, E., Raymond, J. C., Miralles, M. P., & Hara, H. 2010, ApJ, 711, 75
Lario, D., Kallenrode, M.-B., Decker, R. B., et al. 2006, ApJ, 653, 1531
Li, G., Ao, X., Verkhoglyadova, O., Zank, G., & Ding, L. 2012a, in AIP Conf. Proc. 1436, Physics of the Heliosphere: A 10 Year Retrospective, ed. J. Heerikhuisen et al. (Melville, NY: AIP), 178
Li, G., Zank, G. P., & Rice, W. K. M. 2003, JGR, 108, 1082
Li, G., Zank, G., Verkhoglyadova, O., Ao, X., & Ding, L. 2012b, in AIP Conf. Proc. 1500, Space Weather: The Space Radiation Environment, ed. Q. Hu et al. (Melville, NY: AIP), 115
Mewaldt, R. A., Cohen, C. M. S., Giacalone, J., et al. 2008, in AIP Conf. Proc. 1039, Particle Acceleration and Transport in the Heliosphere and Beyond, ed. G. Li et al. (Melville, NY: AIP), 111
Mewaldt, R. A., Cohen, C. M. S., Labrador, A. W., et al. 2005a, JGR, 110, A09S18
Mewaldt, R. A., Cohen, C. M. S., Mason, G. M., et al. 2005b, in Proc. 29th Int. Cosmic Ray Conf. (Pune), 1, 129
Mewaldt, R. A., Cohen, C. M. S., Mason, G. M., et al. 2005c, in Proc. Solar Wind 11-SOHO 16, ed. B. Fleck, T. H. Zurbuchen, & H. Lacoste (ESA SP-592; Noordwijk: ESA), 67
Mewaldt, R. A., Looper, M. D., Cohen, C. M. S., et al. 2012, SSRv, 171, 97
Miyasaka, H., Stone, E. C., Mewaldt, R. A., et al. 2005, in Proc. 29th Int. Cosmic Ray Conf. (Pune), 1, 315
Murphy, N. A., Raymond, J. C., & Korreck, K. E. 2011, ApJ, 735, 17

Patsourakos, S., & Vourlidas, A. 2012, SoPh, 281, 187
Reames, D. V. 1999, SSRv, 90, 413
Reames, D. V. 2013, SSRv, in press
Reames, D. V., & Ng, C. K. 2010, ApJ, 723, 1286
Reames, D. V., Ng, C. K., & Tylka, A. J. 2013, SoPh, 285, 233
Rouillard, A. P., Odstrčil, D., Sheeley, N. R., et al. 2011, ApJ, 735, 7
Rouillard, A. P., Sheeley, N. R., Tylka, A., et al. 2012, ApJ, 752, 44
Smart, D. F., & Shea, M. A. 1992, AdSpR, 12, 303
Smart, D. F., & Shea, M. A. 1995, in Proc. 24th Int. Cosmic Ray Conf. (Rome), 4, 313
Subramanian, P., & Vourlidas, A. 2007, A&A, 467, 685
Tan, L. C., Reames, D. V., & Ng, C. K. 2008, ApJ, 678, 1471
Tan, L. C., Reames, D. V., Ng, C. K., Saloniemi, O., & Wang, L. 2009, ApJ, 701, 1753
Tylka, A. J., Cohen, C. M. S., Dietrich, W. F., et al. 2005, ApJ, 625, 474
Vourlidas, A., Howard, R. A., Esfandiari, E., et al. 2010, ApJ, 722, 1522
Vourlidas, A., Howard, R. A., Esfandiari, E., et al. 2011, ApJ, 730, 59
Vourlidas, A., Subramanian, P., Dere, K. P., & Howard, R. A. 2000, ApJ, 534, 456
Wu, S.-T., Guo, W. P., Andrews, M. D., et al. 1997, SoPh, 175, 719
Yashiro, S., Gopalswamy, N., Akiyama, S., Michalek, G., & Howard, R. A. 2005, JGR, 110, A12S05